ACS APPLIED MATERIALS & INTERFACES

Letter

www.acsami.org

Single-Crystalline 3C-SiC anodically Bonded onto Glass: An Excellent Platform for High-Temperature Electronics and Bioapplications

Hoang-Phuong Phan,*[,†] Han-Hao Cheng,[‡] Toan Dinh,[†] Barry Wood,[‡] Tuan-Khoa Nguyen,[†] Fengwen Mu,[¶] Harshad Kamble,[†] Raja Vadivelu,[†] Glenn Walker,[†] Leonie Hold,[†] Alan Iacopi,[†] Ben Haylock,[§] Dzung Viet Dao,[†] Mirko Lobino,[†,§] Tadatomo Suga,[¶] and Nam-Trung Nguyen[†]

[†]Queensland Micro-Nanotechnology Centre and [§]Centre for Quantum Dynamics, Griffith University, Brisbane, Queensland 4111, Australia

[‡]Australian Institute for Bioengineering and Nanotechnology, The University of Queensland, Brisbane, Queensland 4072, Australia

[¶]Department of Precision Engineering, The University of Tokyo, Tokyo 113-8654, Japan

Supporting Information

ABSTRACT: Single-crystal cubic silicon carbide has attracted great attention for MEMS and electronic devices. However, current leakage at the SiC/Si junction at high temperatures and visible-light absorption of the Si substrate are main obstacles hindering the use of the platform in a broad range of applications. To solve these bottlenecks, we present a new platform of single crystal SiC on an electrically insulating and transparent substrate using an anodic bonding process. The SiC thin film was prepared on a 150 mm Si with a surface roughness of 7 nm using LPCVD. The SiC/Si wafer was bonded to a glass substrate and then the Si layer was completely removed through wafer polishing and wet etching. The bonded SiC/glass samples show a sharp bonding interface of less than 15 nm characterized using deep profile X-ray photoelectron spectroscopy, a strong bonding strength of approximately 20 MPa measured from the pulling test, and relatively high optical transparency in the visible range. The transferred SiC film also exhibited good conductivity and a relatively high temperature coefficient of resistance varying from −12 000 to −20 000 ppm/K, which is desirable for thermal sensors. The biocompatibility of SiC/glass was also confirmed through mouse 3T3 fibroblasts cell-culturing experiments. Taking advantage of the superior electrical properties and biocompatibility of SiC, the developed SiC-on-glass platform offers unprecedented potentials for high-temperature electronics as well as bioapplications.

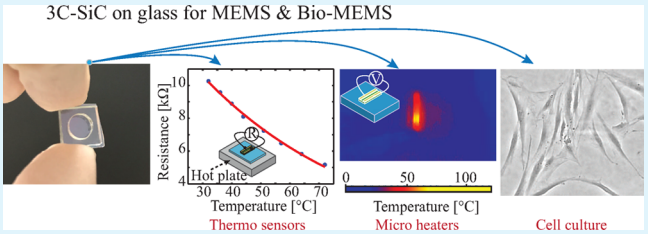

KEYWORDS: *silicon carbide, anodic bonding, MEMS, harsh environment electronics, bioapplications*

Silicon carbide with its superior physical and chemical properties, has been considered a versatile material for a broad range of applications, including high power electronics, high temperature sensors, and bio sensing devices.[1−3] Because of the large energy band gap ranging from 2.3 to 3.4 eV and high breakdown voltage, SiC has been employed in commercial diodes and transistors with an operating voltage ranging from 600 to 1200 V.[4,5] In addition, the thermal stability of SiC also allows the development of sensors for high temperature operations which exceed 500 °C. For example, numerous sensing effects including the piezoresistance and thermoresistance in SiC have been utilized to develop Micro Electromechanical Systems (MEMS) transducers which can be operated in harsh environments.[6−10] Furthermore, because SiC is almost transparent to the visible light and also chemically stable, numerous SiC-based in vivo medical devices have been developed.[11−16] For instance, SiC has been utilized as coating layers for surface passivation of invasive devices,[17] substrates for cell cultures,[18−20] and electrodes for electrochemical devices.[21,22]

Silicon carbide exists in more than 200 poly types.[23,24] Among these, α-SiC (e.g., 4H-SiC, 6H-SiC) and β-SiC are the most well-known crystals. Compared to α-SiC, β-SiC (also known as 3C-SiC) is more favorable for MEMS devices since it can be grown on a Si substrate.[25−27] The use of a Si substrate enables large scale deposition of 3C-SiC thin films, which could significantly reduce the cost of 3C-SiC wafers in comparison to α-SiC. In addition, SiC-on-Si wafers can also be patterned using standard micromachining processes, whereas the fabrication of bulk SiC wafers is relatively challenging due to their chemical inertness. However, current leakage between SiC and Si due to thermal excitation, and plastic deformation of Si prevents the use of SiC/Si at high temperatures.[28,29] A number of attempts have been made to transfer SiC onto different substrates. These attempts have relied on the diffusion bonding (poly Si to poly Si bonding) or thermal bonding (SiO_2 to SiO_2 bonding) to form SiC on insulator wafers (SiCOI of $SiC/SiO_2/Si$).[31−34]

Received: May 11, 2017
Accepted: August 9, 2017
Published: August 9, 2017

DOI: 10.1021/acsami.7b06661
ACS Appl. Mater. Interfaces XXXX, XXX, XXX−XXX

The requirement for an ultrasmooth buffer layer such as SiO_2 formed by sputtering/oxidation and polishing or SiO_2/poly-Si typically complicates the bonding process. In addition, as Si absorbs visible wavelengths, the $SiC/SiO_2/Si$ template eliminates the transparency-advantage of bulk SiC wafers.[30] Furthermore, to date, there has been no report of bonding SiC wafers with diameters above 4 in., which is critical for low-cost and batch fabrication of MEMS devices.

Here we present a new platform of single-crystalline 3C-SiC on glass, which is a transparent and electrical-insulating substrate, formed by the anodic bonding technique. This technique allows direct bonding of large scale wafers with diameters of 6 in. without the requirement for any buffer layer. The fabricated SiC/glass wafer showed a sharp bonding surface characterized using deep profile XPS, as well as good crystallinity measured using Raman spectroscopy. The adhesion strength between the two substrates was also investigated using a pulling test, showing a high tensile strength of 20 MPa. In addition, the excellent electrical insulation of the substrate as well as the transparency of SiC/glass indicate the potential of the developed platform for high-temperature electronic as well as bioapplications.

Single-crystalline 3C-SiC thin films were grown on Si substrates using a low pressure chemical vapor deposition process (LPCVD). Prior to the deposition, Si wafers were cleaned using a standard RCA process. The growth process was then conducted in a hot wall chamber SPT EpiFlx, at a temperature of approximately 1000 °C. Alternating supply epitaxy (ASE) was employed as growth process, with SiH_4 and C_3H_6 as the precursors for Si and C atoms, respectively. Our LPCVD reactor could deposit SiC films on both sides of at least 50 Si wafers in one process (see the Supporting Information). The grown 3C-SiC films exhibited unintentional n-type conductivity, which is considered to be due to the presence of nitrogen residual gas. A detailed description of the SiC thin film characterization can be found elsewhere,[35] where the SiC epilayer was confirmed to be single crystal aligning in [111] directions, based on a θ-2θ Rocking scan. The thicknesses of the films were measured to be approximately 300 nm using NANOMETRICSNanospec/AFT 210. Figure 1a shows an AFM image of a 5 μm × 5 μm area of the as-grown film measured using a noncontact mode with ParkNX20. Accordingly, the surface roughness of the SiC film was found to be approximately 7 nm, which is typically sufficient for a standard anodic bonding process.[36]

The as-grown SiC/Si wafers were then subjected to the anodic bonding process, performed using EVG520IS hot embosser at a pressure between 1.5 and 2.5 kN and bias between −200 to −1000 V. Prior to the bonding step, all wafers were piranha (H_2SO_4:H_2O_2 with a ratio of 3:1) cleaned to reduce surface contamination. The anode electrode was then applied to the SiC/Si wafer while the cathode electrode was connected to the glass wafer (6 in. 1 mm thick Borofloat 33 from University Wafers), Figure 1b. The positive charges in the glass wafer were attracted to the cathode, leaving a depletion layer at the SiC/glass interface. As a result, the oxide negative charges in the glass moved toward the anode and diffused into the SiC to form chemical bonding between the SiC and glass substrate.[37] Figures 1c–e show SiC/Si wafers bonded to glass wafers with different parameters, listed in Table 1. It can be seen that increasing pressure resulted in a larger bonding area. In addition, the plasma treatment using OxfordNGP80 with 50 W RF power, and 20 sccm O_2 flow rate for 60s also significantly

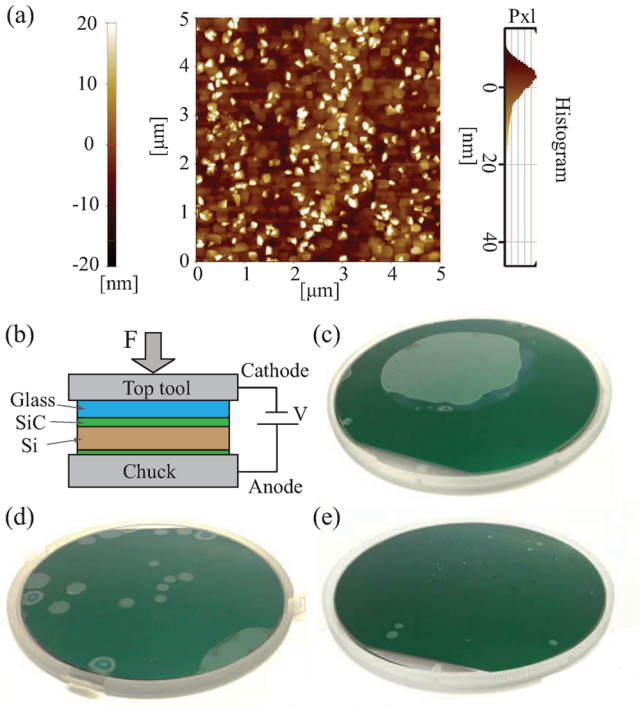

Figure 1. Anodic bonding process. (a) AFM image of a SiC film prior to bonding; (b) configuration of the bonding process; (c–e) photograph of wafers bonded with different parameters.

Table 1. Bonding Parameters of SiC/Si Wafers to Glass Wafers

sample number	cleaning	O_2 plasma	voltage step (V)	HT time (min)	piston force (N)
1	yes	no	−200/−400/−600	10/10/20	1500
2	yes	no	−200/−400/−600/−800	5/5/10/20	2500
3	yes	yes	−200/−500/−700/−1000	5/5/10/20	2500

enhances the bonding surface of the wafers. As such, using a high pressurized force of approximately 2.5 kN and the O_2 plasma treatment, 98% of the SiC surface area was successfully bonded to the glass surface. There was no crack and no significant wafer bow in the bonded 150 mm-diameter wafers.

To form SiC on insulator (i.e., glass), the top Si layer was completely removed using the mechanical polishing followed by wet etching. In the mechanical polishing step, the pressure applied to the Si/SiC/glass sample was set at approximately 170 kPa, whereas the rotational speed was 40 rpm. The Si removal rate was measured at 10 μm/min with a calcined aluminum oxide powder. The polishing process was stopped once the thickness of Si layer reached 5 to 10 μm, and then the remaining Si was completely removed using wet etching in a HNA solution ($HF:HNO_3:CH_3COOH$ with a ratio of 2:2:3) at room temperature. Because of its chemical inertness, SiC was not attacked by HNA solution. Figure 2a shows a bonded Si/SiC/glass chip, and a SiC/glass sample after Si removal. It should also be pointed out that the SiC films bonded to glass substrate was reflected with respect to the original SiC films on Si wafers. This means that, the high-density-of-defect SiC layer at the vicinity of the initial SiC and Si interface[38] is on the top surface after bonding and Si-removing. Subsequently, this

DOI: 10.1021/acsami.7b06661
ACS Appl. Mater. Interfaces XXXX, XXX, XXX−XXX

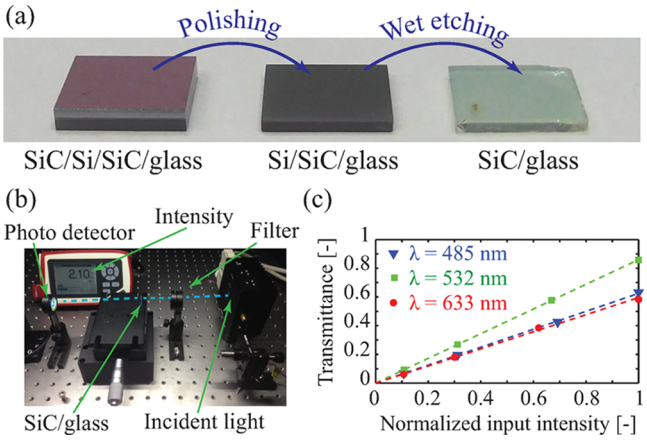

Figure 2. (a) Fabrication of SiC/glass chip (It should be noted that since SiC was deposited on both sides of a Si wafer, the initial configuration of the bonded chip was SiC/Si/SiC/glass. The top SiC layer and the Si layer underneath were then removed using wafer polishing). (b) Setup for transmittance measurement. (c) Transmittance of SiC/glass measured at different wavelengths of 485, 532, and 633 nm, respectively.

highly density defect layer could be simply removed using a top-down etching process, improving the uniformity and quality of bonded SiC layer. Further investigation into the electrical properties of SiC/glass before and after removing the high density of defect layer will be carried out in the future work.

SiC/glass exhibits excellent transparency at visible wavelengths. The optical transmittance of the SiC/glass was measured using the experimental setup shown in Figure 2(b), where the intensity of transmitted light through SiC/glass was monitored using a photo detector. Experimental data show that the SiC/glass film exhibits relatively large transmittance of 63%, 86%, and 60% at wavelengths of 485 nm (blue), 532 nm (green), and 633 nm (red), respectively, as shown in Figure 2c. In addition, the dependence of the transmittance on different wavelength also indicates the possibility of using this new platform for optical filtering applications.

The X-ray photoelectron spectroscopy (XPS) analysis of the bonded wafer was performed using a KratosAXIS Ultra under ultrahigh vacuum conditions, where the X-ray radiation was generated from a monochromatic Al X-ray source at 225 W. Ar ions were utilized to etch the layers of interest with an etching rate of 1.92 nm/min for SiC and 3.6 nm/min for the glass layer. Figure 3a shows a 3D-plot of the XPS depth profile of a 100 μm × 100 μm area, after a total etching time of 10,000 s. The layer=by=layer XPS survey scan was performed for each 100 s etching cycle, showing the binding energies of the constructing element (e.g., Si, C, O). The profile of each layer can also be differentiated from the binding energy with its corresponding atomic concentration. The similarity of the binding energies peaks also indicates the uniformity of the films (e.g., the SiC films plotted with the blue curves). Figure 3b–e show the XPS spectra of the top layer, the bulk SiC layer, the SiC/SiO2 interface, and the bulk SiO2 layer, respectively, which were extracted from Figure 3a. Accordingly, a binding energy peak at 530 meV corresponding to the oxide element was found in the top layer of the SiC film (less than 3 nm), indicating that the SiC film was slightly oxidized (see Figure 3b). However, when removing the top layer through the first Ar ion bombardment step, the peak at 530 eV disappeared, and only Si and C element was detected in the bulk SiC layer. When the ion etching reaches the interface, all O 1s (530 eV), C 1s (285 eV), and Si 2p (100 eV) peaks were clearly observed (see Figure 3d). Finally, when etching through SiC layer and deep into the SiO_2 layer, the binding energy at 285 eV corresponding to C 1s disappeared, leaving the peaks corresponding to Si and O elements. Furthermore, from the atomic concentration of elements against the etching depth plotted in Figure 3e, the thickness of the bonding interface was found to be less than 15 nm, which is much smaller than that of the SiC films on glass

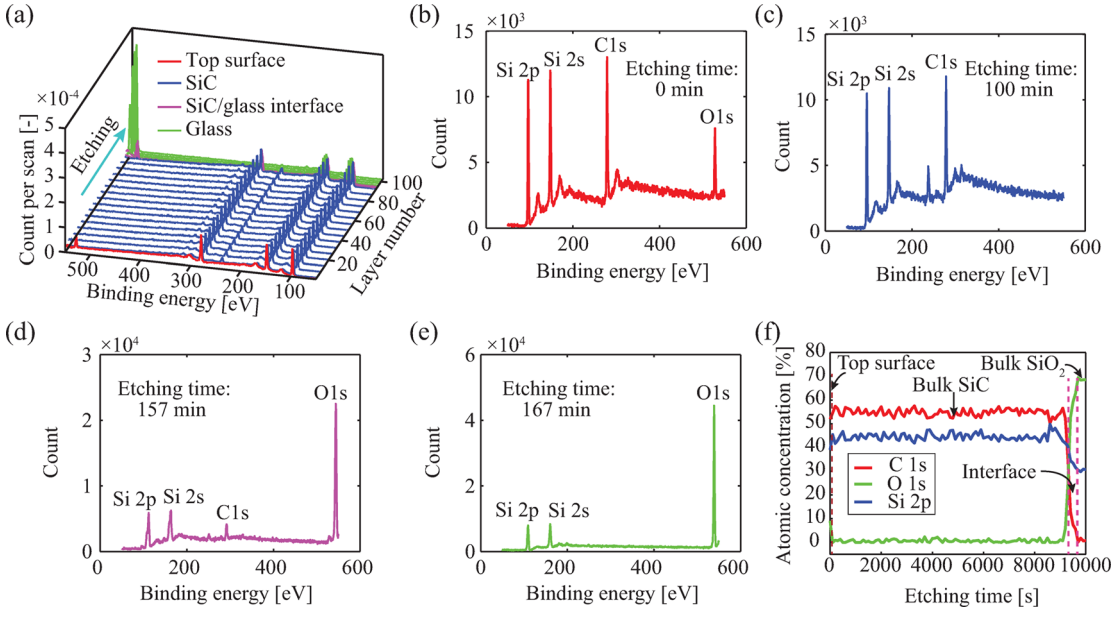

Figure 3. Depth profile X-ray photoelectron spectroscopy of the bonded SiC/glass sample. (a) 3D plot of the XPS along the deepness of the SiC films; XPS survey spectra for different layers: (b) top SiC surface, (c) SiC film, (d) interface and (e) bulk glass; (f) atomic contribution of Si, C, and O.

DOI: 10.1021/acsami.7b06661
ACS Appl. Mater. Interfaces XXXX, XXX, XXX−XXX

substrates. The thin bonding area is favorable because it is expected not to induce significant damage into the entire film.

The crystallinity of the SiC films was also investigated using Raman scattering with a RenishawinVia Raman microscope at a wavelength of 514 nm. Figure 4 shows the Raman shift of the

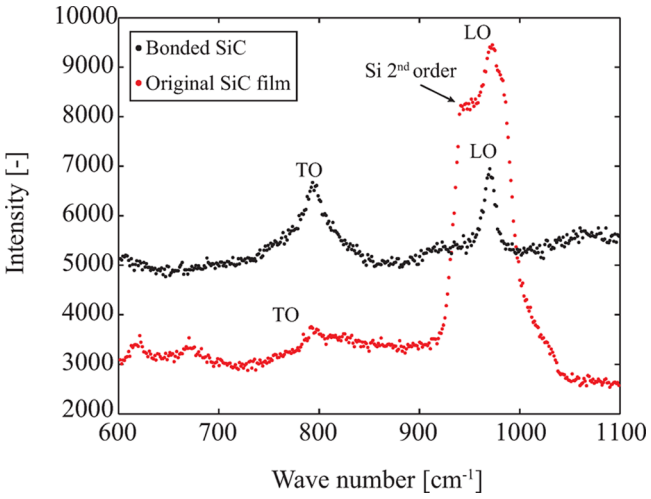

Figure 4. Raman spectroscopy of prebonding and bonded SiC films.

SiC film before and after bonding (with Si layer being removed). For the SiC film grown on Si substrate a transverse optical phonon peak at 796 cm^{-1} and a longitudinal optical phonon at 960 cm^{-1} was observed. However, the LO peak was relatively broad which is considered to be caused by the influence of the silicon second phonon peak at 950 cm^{-1}. This effect typically causes the signal obtained from the LO peak of the epitaxial 3C-SiC to be less informative for film analysis. In the transferred film, both TO and LO peaks were clearly observed, indicating a good crystallinity. In addition, since the Si layer was removed, the influence of the Si substrate on the SiC layer was completely eliminated. The sharp TO and LO peaks in the transferred film effectively enable further investigation into the properties of films (e.g., residual strain, and thermally induced strain) which can be performed using the Raman shift.

The bonding strength between SiC and glass was evaluated by a pulling test with a tensile pulling machine ShimadzuAG-X (see Figure 5a). In this experiment, Si/SiC/glass chips with a surface area of 10 mm × 10 mm were attached to the copper jigs of the pulling tester by epoxy as shown in Figure 5b. The applied tensile stress was recorded until the sample reached the fracture point. Experimental data showed that the tensile strength of all samples ranged from 20 to 25 MPa. It should be noted that, the fracture surface occurred in the glass layer, indicating that the tensile strength of the anodic bonding between SiC and glass could be well above the tensile strength of glass. Our data are in good agreement with those reported for anodic bonding of Si wafers.[39] The result indicates the excellent bond strength of SiC/glass interface, which is suitable for the development of MEMS mechanical sensors.

The transferred SiC films with their high optical transmittance and mechanically strong bonds are ideal for MEMS sensing applications. The following experiments were carried out to demonstrate SiC/glass as thermo-based sensors utilizing the thermoresistive effect of the SiC films. A 200 nm Ni layer was sputtered (using SurreyNanoSystems-γ) and then

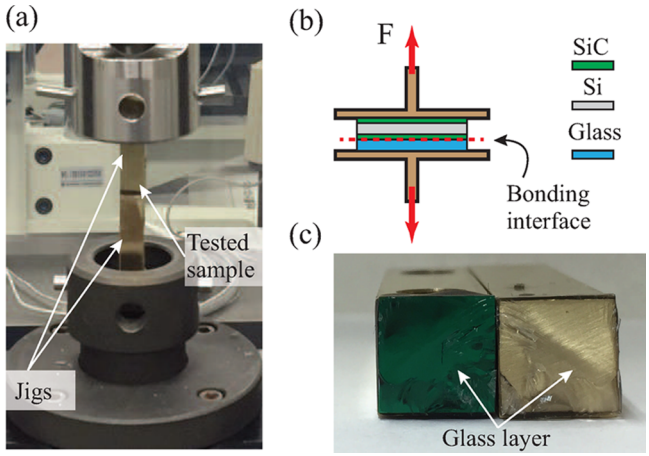

Figure 5. Evaluation of bonding strength by pulling test. (a) Schematic sketch of experiment setup; (b, c) Fracture surfaces occurred in the epoxy and glass layers, respectively.

patterned using lift-off (photoresist AZ6612) to form electrical contact with the transferred SiC films. Figure 6a shows the current−voltage (I−V) curves of SiC resistors with a width of 10 mm, while the length varying from 1 to 3 mm, measured using a power device analyzer AgilentB1505A. The linearity between the applied voltage and the measured current indicated that a good Ohmic contact was formed between Ni and n-type SiC. The proportion of the current and the length of the SiC resistors also indicates a low resistance contact of below 100 Ω using the transmission line method. Because glass is an excellent insulating material, the current leakage from SiC to the substrate was found to be extremely low; below 10 pA at room temperature and up to 300 °C. In addition, the resistance of SiC films returned to its initial value after several heating cycles (where the temperature was increased to 300 °C and then returned to 25 °C). The excellent long-term stability of SiC resistance at high temperatures is attributed to its extremely low oxidation rate in comparison to that of Si (see the Supporting Information). Furthermore, no crack was generated in the SiC films throughout the heating and cooling experiments, indicating its mechanical robustness for high-temperature applications.

The SiC on glass was patterned into resistors which can perform as a highly sensitive thermal sensor. The relationship between temperature and resistance changes of n-type 3C-SiC was plotted in Figure 6b. Evidently, the resistance of the n-type 3C-SiC significantly decreased with increasing temperature. This result is attributed to the fact that the conduction of the n-type SiC film was thermally activated because of the ionization of impurities, leading to an increase in the carrier concentration.[40] The magnitude of the thermoresistive effect of n-type 3C-SiC can also be quantified using the temperature coefficient of resistance (TCR): $TCR = (\Delta R/R_0)/\Delta T$. As shown in Figure 6c, the TCR of the transferred film was found to be −20 000 ppm/K at room temperature and dropped to −12 000 ppm/K at 70 °C. This TCR is comparable to that of amorphous Si but the thermoresistance of transferred SiC offers several advantages over Si.[41] As such, the SiC resistance exhibits excellent temperature-stability under visible light due to its large optical band gap of 2.94 to 3.5 eV in comparison to the photon energy in the visible range of 2 to 2.5 eV. This allows SiC/glass-based temperature sensors operating under visible

DOI: 10.1021/acsami.7b06661
ACS Appl. Mater. Interfaces XXXX, XXX, XXX−XXX

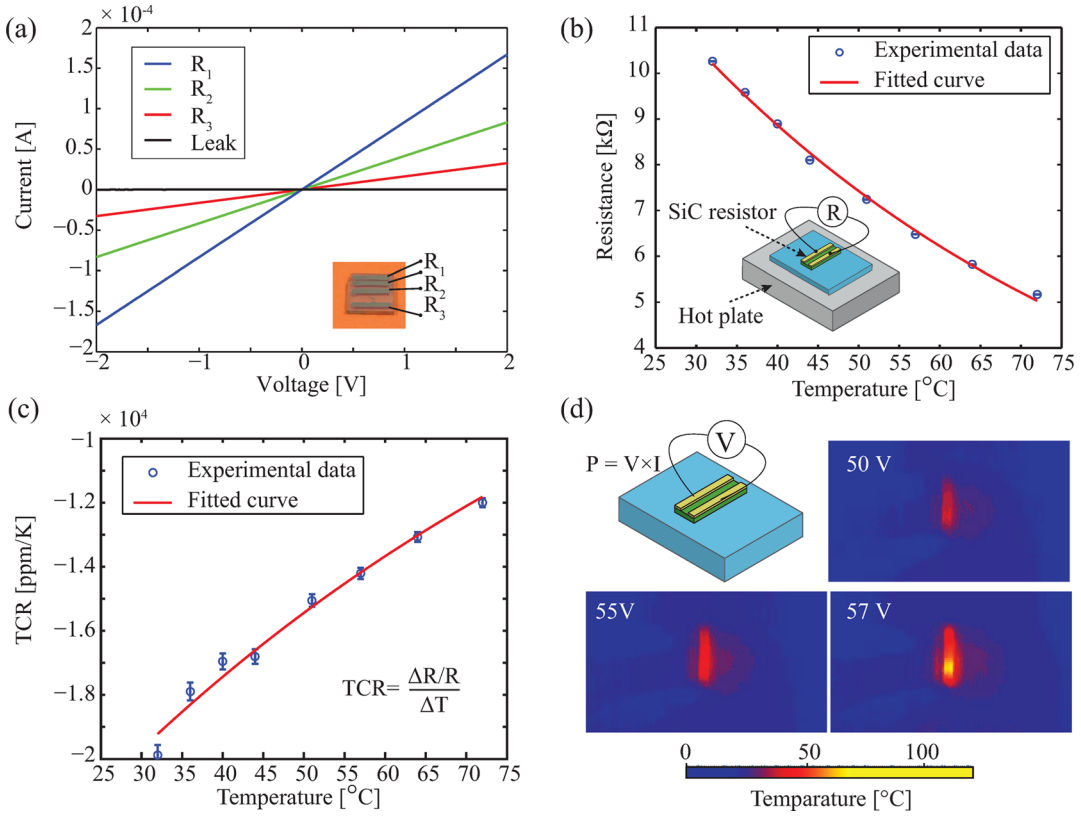

Figure 6. Electrical properties of the bonded films. (a) IV characteristic; (b) change of resistance against temperature; (c) temperature coefficient of resistance; (d) Demonstration of SiC/glass heater.

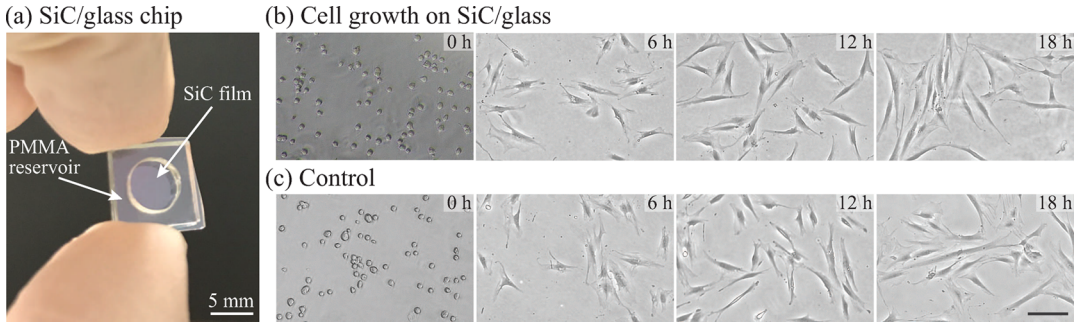

Figure 7. Cell morphology and growth on the SiC surface. (a) Photograph of a SiC/glass chip with a PMMA reservoir. Cell growth with (b) the SiC/glass template and (c) control, showing that 6 h after cell seeding, cells were attached onto the surface. After 12 and 18 h, further adherence and cell-to-cell contact was observed. Scale bar: 100 μm.

light illumination (e.g., microscope) without the requirement for photon compensation.[42]

As well as temperature sensing, the transferred film can also be used as a heater for bioapplications such as thermal therapy devices. The elimination of the leakage current to the glass substrate enables the application of a large current through a SiC resistor, generating relatively high temperatures caused by the Joule heating effect. As a proof of concept, we applied relatively high voltage to the SiC resistor with dimensions of 10 mm × 1 mm. The temperature distribution on the SiC heater obtained from an IR camera demonstrated the capability of generating the temperature of SiC above 100 °C with a sufficiently high voltage (e.g., 57 V). It is also evident that the temperature of the heater is controllable by varying the applied voltages.

The biocompatibility of the SiC/glass platform was demonstrated in the following cell culturing experiments. A PMMA reservoir with a diameter of 6 mm was attached to a SiC/glass chip with dimensions of 10 mm × 10 mm, as shown in Figure 7a. The transparency of the SiC/glass chip enables observation of cell growth under a typical inverted optical microscopy. Prior to cell culturing, the surface of SiC was cleaned and treated with ethanol and UV exposure. Subsequently, mouse 3T3 fibroblasts cells were grown on SiC surface and a standard cell culture dish for comparison. A detailed description of the methodology used for cell culture and imaging is presented in the Supporting Information. Figure 7b shows the growth and adhesion of the fibroblast cells on the SiC substrate for every 6 h within a period of 18 h using a NikonEclipseTs2 microscope. Phase contrast imaging of cells, over 6 h culturing on the SiC film showed that fibroblast cells

DOI: 10.1021/acsami.7b06661
ACS Appl. Mater. Interfaces XXXX, XXX, XXX−XXX

closely attached to the SiC surface. After 12 h, the healthier cell adhesion was observed and cell morphology appeared to be the typical fibroblast. Evidently, these cells extensively spread their cytoplasmic projection, which is important to anchor them to the SiC surface. As expected, after 18 h, cells were able to sustain adherence and established contact with neighboring cells. Similar observations were also recorded in cells grown in a standard cell culture dish, which is represented as a control surface, as illustrated in Figure 7c. The resulting morphologies and cell behavior reveal the cyto-compatibility of the SiC substrate as well as its potential for the integration of electronics and cell culture.

In conclusion, we demonstrated for the first time the large-scale transfer of a single-crystalline 3C-SiC thin film on an electrically insulating and optically transparent glass substrate, using anodic bonding. The bonded SiC films show excellent crystal quality and relatively sharp bonding interface with an excellent adhesion between the SiC and glass, which is suitable for MEMS mechanical sensors. The good electrical conductivity, stability under visible light, relatively high TCR, and biocompatibility making the developed SiC on glass a promising platform for future development of not only high-temperature sensing and electronics but also bioapplications.

■ ASSOCIATED CONTENT

Supporting Information

The Supporting Information is available free of charge on the ACS Publications website at DOI: 10.1021/acsami.7b06661.

Detailed experimental procedures of the LPCVD process, plasma assisted wafer bonding, measurement of optical transmittance, the fabrication of SiC resistors, the oxidation test of SiC and Si, and the methodology for cell culture (PDF)

■ AUTHOR INFORMATION

Corresponding Author

*E-mail: hoangphuong.phan@griffithuni.edu.au.

ORCID

Hoang-Phuong Phan: 0000-0002-1724-5667
Toan Dinh: 0000-0002-7489-9640
Tuan-Khoa Nguyen: 0000-0003-1271-9576

Notes

The authors declare no competing financial interest.

■ ACKNOWLEDGMENTS

This work was partially funded by the linkage grant (LP150100153) and discovery project (DP140100808) from the Australian Research Council (ARC). This work was performed in part at the Queensland node of the Australian National Fabrication Facility, a company established under the National Collaborative Research Infrastructure Strategy to provide nano and microfabrication facilities for Australia's researchers. B.H. acknowledges support through an Australian Government Research Training Program Scholarship. The authors acknowledge Dr. Philip Tanner for valuable discussion on thin SiC films deposition.

■ REFERENCES

(1) Eddy, C. R.; Gaskill, D. K. Silicon Carbide as a Platform for Power Electronics. *Science* **2009**, *324*, 1398−1400.

(2) Phan, H.-P.; Dao, D. V.; Nakamura, K.; Dimitrijev, S.; Nguyen, N.-T. Piezoresistive Effect in Silicon Carbide for High Temperature Sensors: A Review. *J. Microelectromech. Syst.* **2015**, *24*, 1663−1677.

(3) Senesky, D. G.; Jamshidi, B.; Cheng, K. B.; Pisano, A. P. Harsh Environment Silicon Carbide Sensors for Health and Performance Monitoring of Aerospace Systems: a Review. *IEEE Sens. J.* **2009**, *9*, 1472−1478.

(4) Rabkowski, J.; Peftitsis, D.; Nee, H. P. Silicon Carbide Power Transistors: A New Era in Power Electronics Is Initiated. *IEEE Ind. Electron. Mag.* **2012**, *6*, 17−26.

(5) Nakamura, D.; Gunjishima, I.; Yamaguchi, S.; Ito, T.; Okamoto, A.; Kondo, H.; Onda, S.; Takatori, K. Ultrahigh-Quality Silicon Carbide Single Crystals. *Nature* **2004**, *430*, 1009−1012.

(6) Qamar, A.; Phan, H.-P.; Dao, D. V.; Tanner, P.; Dinh, T.; Wang, L.; Dimitrijev, S. The Dependence of Offset Voltage in P-Type 3C-SiC Van der Pauw Device on Applied Strain. *IEEE Electron Device Lett.* **2015**, *36*, 708−710.

(7) Dao, D. V.; Phan, H.-P.; Qamar, A.; Dinh, T. Piezoresistive Effect of P-Type Single Crystalline 3C-SiC on (111) Plane. *RSC Adv.* **2016**, *6*, 21302−21307.

(8) Gao, F.; Zheng, J.; Wang, M.; Wei, G.; Yang, W. Piezoresistance Behaviors of P-Type 6H-SiC Nanowires. *Chem. Commun.* **2011**, *47*, 11993−11995.

(9) Wright, N. G.; Horsfall, A. B.; Vassilevski, K. Prospects for SiC Electronics and Sensors. *Mater. Today* **2008**, *11*, 16−21.

(10) Dinh, T.; Phan, H.-P.; Kozeki, T.; Qamar, A.; Namazu, T.; Nguyen, N.-T.; Dao, D.-V. Thermoresistive Properties of P-Type 3C-SiC Nanoscale Thin Films for High-Temperature MEMS Thermal-based Sensors. *RSC Adv.* **2015**, *5*, 106083−106086.

(11) Yang, T.; Zhang, L.; Hou, X.; Chen, J.; Chou, K. C. Bare and Boron-Doped Cubic Silicon Carbide Nanowires for Electrochemical Detection of Nitrite Sensitively. *Sci. Rep.* **2016**, *6*, 24872.

(12) Saddow, S. E. Silicon Carbide Biotechnology: A Biocompatible Semiconductor for Advanced Biomedical Devices and Applications. *Elsevier* **2012**, 1.

(13) Naglieri, V.; Gludovatz, B.; Tomsia, A. P.; Ritchie, R. O. Developing Strength and Toughness in Bio-Inspired Silicon Carbide Hybrid Materials Containing a Compliant Phase. *Acta Mater.* **2015**, *98*, 141−151.

(14) Sanger, A.; Jain, P. K.; Mishra, Y. K.; Chandra, R. Palladium Decorated Silicon Carbide Nanocauliflowers for Hydrogen Gas Sensing Application. *Sens. Actuators, B* **2017**, *242*, 694−699.

(15) Schoell, S. J.; Sachsenhauser, M.; Oliveros, A.; Howgate, J.; Stutzmann, M.; Brandt, M. S.; Frewin, C. L.; Saddow, S. E.; Sharp, I. D. Organic Functionalization of 3C-SiC Surfaces. *ACS Appl. Mater. Interfaces* **2013**, *5*, 1393−1399.

(16) Huang, H.; Wong, S. L.; Sun, J.; Chen, W.; Wee, A. T. S. Trapping Single Polar Molecules in SiC Nanomesh via out-of-Plane Dipoles. *ACS Nano* **2012**, *6*, 2774−2778.

(17) Heublein, B.; Pethig, K.; Elsayed, A. M. Silicon Carbide Coating NA Semiconducting Hybrid Design of Coronary Stents NA Feasibility Study. *J. Invasive Cardiol.* **1998**, *10*, 255−262.

(18) Lanzani, G. Materials for bioelectronics: Organic Electronics Meets Biology. *Nat. Mater.* **2014**, *13*, 775−776.

(19) Fradetal, L.; Bano, E.; Attolini, G.; Rossi, F.; Stambouli, V. A Silicon Carbide Nanowire Field Effect Transistor for DNA Detection. *Nanotechnology* **2016**, *27*, 235501.

(20) Fan, J.; Li, H.; Jiang, J.; So, L. K.; Lam, Y. W.; Chu, P. K. 3C-SiC Nanocrystals as Fluorescent Biological Labels. *Small* **2008**, *4*, 1058−1062.

(21) Zhuang, H.; Yang, N.; Zhang, L.; Fuchs, R.; Jiang, X. Electrochemical Properties and Applications of Nanocrystalline, Microcrystalline, and Epitaxial Cubic Silicon Carbide Films. *ACS Appl. Mater. Interfaces* **2015**, *7*, 10886−10895.

(22) Shi, C.; Wei, C.; Han, H.; Xingyu, G.; Dongchen, Q.; Yuzhan, W.; Wee, A. T. S. Template-Directed Molecular Assembly on Silicon Carbide Nanomesh: Comparison Between CuPc and Pentacene. *ACS Nano* **2010**, *4*, 849−854.

DOI: 10.1021/acsami.7b06661
ACS Appl. Mater. Interfaces XXXX, XXX, XXX−XXX

(23) Madar, R. Materials Science: Silicon Carbide in Contention. *Nature* **2004**, *430*, 974−975.
(24) Phan, H. P.; Dinh, T.; Kozeki, T.; Qamar, A.; Namazu, T.; Dimitrijev, S.; Nguyen, N.-T.; Dao, D. V. Piezoresistive Effect in P-Type 3C-SiC at High Temperatures Characterized using Joule Heating. *Sci. Rep.* **2016**, *6*, 28499.
(25) Lu, X.; Lee, J. Y.; Feng, P. X. L.; Lin, Q. Silicon Carbide Microdisk Resonator. *Opt. Lett.* **2013**, *38*, 1304−1306.
(26) Phan, H.-P.; Nguyen, T. K.; Dinh, T.; Ina, G.; Kermany, A. R.; Qamar, A.; Han, J.; Namazu, T.; Maeda, R.; Dao, D. V.; Nguyen, N.-T. Ultra-High Strain in Epitaxial Silicon Carbide Nanostructures Utilizing Residual Stress Amplification. *Appl. Phys. Lett.* **2017**, *110*, 141906.
(27) Wang, Z.; Lee, J.; Feng, P. X. L. Spatial Mapping of Multimode Brownian Motions in High-Frequency Silicon Carbide Microdisk Resonators. *Nat. Commun.* **2014**, *5*, 5158.
(28) Adachi, K.; Watanabe, N.; Okamoto, H.; Yamaguchi, H.; Kimoto, T.; Suda, J. Single-Crystalline 4H-SiC Micro Cantilevers with a High Quality Factor. *Sens. Actuators, A* **2013**, *197*, 122−125.
(29) Placidi, M.; Perez-Tomas, A.; Zielinski, M.; Godignon, P.; Millan, J.; Jorda, X.; Mestres, N.; Abadal, G. 3C-SiC Films on Insulated Substrates for High-Temperature Electrostatic-based Resonators. *J. Micromech. Microeng.* **2010**, *20*, 115007.
(30) Oliveros, A.; Guiseppi-Elie, A.; Saddow, S. E. Silicon Carbide: A Versatile Material for Biosensor Applications. *Biomed. Microdevices* **2013**, *15*, 353−368.
(31) Serre, C.; Romano-Rodriguez, A.; Perez-Rodriguez, A.; Morante, J. R.; Fonseca, L.; Acero, M. C.; Kogler, R.; Skorupa, W. β-SiC on SiO_2 Formed by Ion Implantation and Bonding for Micromechanics Applications. *Sens. Actuators, A* **1999**, *74*, 169−173.
(32) Suga, T.; Mu, F.; Fujino, M.; Takahashi, Y.; Nakazawa, H.; Iguchi, K. Silicon Carbide Wafer Bonding by Modified Surface Activated Bonding Method. *Jpn. J. Appl. Phys.* **2015**, *54*, 030214.
(33) Wu, C.-H.; Zorman, C. A.; Mehregany, M. Fabrication and Testing of Bulk MicromachinedSilicon Carbide Piezoresistive Pressure Sensors for High Temperature Applications. *IEEE Sens. J.* **2006**, *6*, 316.
(34) Vinod, K. N.; Zorman, A. A.; Yasseen, A. A.; Mehregany, M. Fabrication of Low Defect Density 3C-SiC on SiO_2 Structures Using Wafer Bonding Techniques. *J. Electron. Mater.* **1998**, *27*, L17−L20.
(35) Qamar, A.; Dao, D. V.; Han, J.; Phan, H.-P.; Younis, A.; Tanner, P.; Dinh, T.; Wang, L.; Dimitrijev, S. Pseudo-Hall Effect in Single Crystal 3C-SiC(111) Four-Terminal Devices. *J. Mater. Chem. C* **2015**, *3*, 12394−12398.
(36) Wei, J.; Xie, H.; Nai, M. L.; Wong, C. K.; Lee, L. C. Low Temperature Qafer Anodic Bonding. *J. Micromech. Microeng.* **2003**, *13*, 217.
(37) Kim, H. S.; Blick, R. H.; Kim, D. M.; Eom, C. B. Bonding Silicon-on-Insulator to Glass Wafers for Integrated Bio-Electronic Circuits. *Appl. Phys. Lett.* **2004**, *85*, 2370−2372.
(38) Song, X.; Michaud, J. F.; Cayrel, F.; Zielinski, M.; Portail, M.; Chassagne, T.; Collard, E.; Alquier, D. Evidence of Electrical Activity of Extended Defects in 3C-SiC Grown on Si. *Appl. Phys. Lett.* **2010**, *96*, 142104.
(39) Lee, T. M. H.; Lee, D. H. Y.; Liaw, C. Y. N.; Lao, A. I. K.; Hsing, I.-M. Detailed Characterization of Anodic Bonding Process between Glass and Thin-Film Coated Silicon Substrates. *Sens. Actuators, A* **2000**, *86*, 103−107.
(40) Kim, K. K.; Kim, H. S.; Hwang, D. K.; Lim, J. H.; Park, S. J. Realization of P-Type ZnO Thin Films via Phosphorus Doping and Thermal Activation of the Dopant. *Appl. Phys. Lett.* **2003**, *83*, 63−65.
(41) Dinh, T.; Phan, H. P.; Kozeki, T.; Qamar, A.; Fujii, T.; Namazu, T.; Nguyen, N. T.; Dao, D. V. High Thermosensitivity of Silicon Nanowires Induced by Amorphization. *Mater. Lett.* **2016**, *177*, 80−84.
(42) Jung, U. G.; Kuwana, K.; Ajiki, Y.; Takahashi, H.; Kan, T.; Takei, Y.; Noda, K.; Iwase, E.; Matsumoto, K.; Shimoyama, I. A photo-response-Compensated Parallel Piezoresistive Cantilever for Cellular Force Measurements. *J. Micromech. Microeng.* **2013**, *23*, 045015.

DOI: 10.1021/acsami.7b06661
ACS Appl. Mater. Interfaces XXXX, XXX, XXX−XXX